Optica Applicata VIII/4, 1978

*T. Araki, T. Asakura**

Apodized images of coherently illuminated edges in the presence of defocusing and spherical aberration

Apodized images of coherently illuminated edges in the presence of defocusing and primary spherical aberration are studied for the apodized pupils of three different types in comparison with non-apodized edge images. The resultant apodized images are evaluated from the edge ringing and shifting phenomena that usually occur in any images of coherently illuminated edges without the operation of apodized.

1. Introduction

There are three major effects in coherent imagery that are characterized by edge ringing, edge shifting, and speckling [1]. Among them, the edge ringing phenomenon has recently received special attention of two groups [2–9] at Imperial College and University of Rochester from the viewpoint of apodization in coherent imagery. Very recently, ASAKURA and ARAKI [10–12] have performed the apodization study of removing or reducing the edge ringing phenomenon by considering another major effect of edge shifting in coherent imagery. Those studies [2–12] are conducted by assuming a coherent optical imaging system to be aberration-free. In an actual optical system, however, there usually exist some aberrations. As a result, both edge ringing and edge shifting phenomena are more highly enhanced in the aberrated optical imaging system than in the aberration-free one. Therefore, the coherent apodization study of removing the edge ringing phenomenon with the consideration of reducing the edge shifting phenomenon should be investigated in the aberrated optical imaging system. This paper studies the apodized images of coherently illuminated edges in the presence of defocusing and primary spherical aberration. The resultant apodized images are evaluated from the edge ringing and shifting phenomena that always occur in any images of coherently illuminated edges without the operation of apodization.

It should be pointed out that the non-apodized images of coherently illuminated edges in the presence of aberrations have been studied in some detail by BARAKAT [13] and ROWE [14].

* Research Institute of Applied Electricity, Hokkaido University, Sapporo, Hokkaido, Japan.

2. General consideration

The complex amplitude of a point object at the image plane (x, y) which is called an amplitude point spread function of an optical imaging system is connected to the pupil function $T(u, v)$ as

$$F(x, y) = \int_{-\infty}^{\infty}\int T(u, v)\exp\{i(xu+yv)\}\,du\,dv \qquad (1)$$

where u and v stand for the relative coordinates having the relation

$$u = (2\pi/\lambda)\,\xi n\sin\alpha,$$

$$v = (2\pi/\lambda)\;\eta\sin\alpha$$

in which λ is the wavelength of light in vacum, n is the refractive index, α is the convergence angle with respect to the optical axis, and ξ and η are the geometrical coordinates of the point at the exit pupil. The edge of the pupil is given by $(u^2+v^2)^{1/2} = 1$. By denoting $U_0(x', y')$ for the complex amplitude distribution of an extended object at the object plane (x', y'), the amplitude distribution $U_i(x, y)$ of its image is expressed by a convolution of $U_0(x', y')$ with the amplitude point spread function $F(x-x', y-y')$, i.e.

$$U_i(x, y) = \int_{-\infty}^{\infty}\int F(x-x', y-y')\,U_0(x', y')\,dx'\,dy' \qquad (2)$$

where it has been tacitly assumed that the isoplanatic condition holds. By means of Fourier transform relationships, eq. (2) can be written as

$$\tilde{U}_i(u, v) = \tilde{U}_0(u, v)T(u, v) \qquad (3)$$

where $\tilde{U}_0$, $\tilde{U}_i$ and T designate the Fourier transforms of U_0, U_i and F, i.e.

$$\tilde{U}_0(u, v) = \int_{-\infty}^{\infty}\int U_0(x, y)\exp\{-i(ux+vy)\}\,dx\,dy, \qquad (4a)$$

$$\tilde{U}_i(u, v) = \int\int_{-\infty}^{\infty} U_i(x, y)\exp\{-i(ux+vy)\}dxdy, \quad (4b)$$

$$T(u, v) = \int\int_{-\infty}^{\infty} F(x, y)\exp\{-i(ux+vy)\}dxdy. \quad (4c)$$

The pupil function $T(u, v)$ of the optical imaging system having aberrations may be expressed by

$$T(u, v) = T_0(u, v)\exp\{i\Phi(u, v)\} \quad (5)$$

where $T_0(u, v)$ denotes the amplitude transmittance over the pupil and $\Phi(u, v)$ indicates the wave aberration function of the system. $T_0(u, v)$ is taken to be equal to unity when the operation of apodization is not considered.

A coherently illuminated edge object is described in amplitude [15] as

$$U_0(x', y') = \frac{1}{2}(1+\mathrm{sgn}x') \quad (6)$$

where

$$\mathrm{sgn}x' = \frac{x'}{|x'|} = \begin{cases} 1, & x' > 0 \\ -1, & x' < 0. \end{cases}$$

A Fourier transform of the edge object given by eq. (6) is given by

$$\tilde{U}_0(u, v) = \frac{1}{2\pi}\left\{\pi\delta(u)+\frac{1}{iu}\right\}\delta(v) \quad (7)$$

where δ is a Dirac delta function. Substitution of eqs. (5) and (7) into eq. (3) gives the image amplitude spectrum $\tilde{U}_i(u, v)$ from which the complex amplitude of the edge image at the image plane is obtained from eq. (4b) as

$$U_i(x, y) = \frac{1}{2\pi}\int\int_{-\infty}^{\infty}\left\{\pi\delta(u)+\frac{1}{iu}\right\}\delta(v)T_0(u, v)\exp\{i\Phi(u, v)\}\times \times\exp\{i(xu+yv)\}dudv. \quad (8)$$

The integration of eq. (8) is performed only within the pupil because the pupil function given by $T(u, v)$ vanishes outside the pupil. After some manipulation in the integration of eq. (8) using the shifting property of the Dirac delta function.

Eq. (8) becomes

$$U_i(x) = \frac{T_0(0)}{2} + \frac{1}{2\pi}\int_{-1}^{1} T_0(u)\cos\{\Phi(u)\}\frac{\sin(xu)}{u}du + + \frac{i}{2\pi}\int_{-1}^{1} T_0(u)\sin\{\Phi(u)\}\frac{\sin(xu)}{u}du. \quad (9)$$

In deriving eq. (9), the wave aberration function $\Phi(u)$ and the amplitude transmittance $T_0(u)$ have been assumed to be even functions. The intensity distribution of an edge image is then given by the absolute square of eq. (9), i.e.

$$I(x) = |U_i(x)|^2 = \left[\frac{1}{2} + \frac{1}{2\pi}\int_{-1}^{1} T_0(u)\cos\{\Phi(u)\}\frac{\sin(xu)}{u}du\right]^2 + + \left[\frac{1}{2\pi}\int_{-1}^{1} T_0(u)\sin\{\Phi(u)\}\frac{\sin(xu)}{z}du\right]^2 \quad (10)$$

where the central transmittance of the pupil function has been assumed to be $T_0(0) = 1$. When the optical system is aberration-free, $\Phi(u) = 0$, eq. (10) reduces to the familiar expression

$$I(x) = \left\{\frac{1}{2} + \frac{1}{2\pi}\int_{-1}^{1} T_0(u)\frac{\sin(xu)}{u}du\right\}^2 \quad (11)$$

which is well known for giving the intensity distribution of a perfectly focused edge image produced under illumination of the completely coherent light.

As a measure of the edge shift which has been introduced by the present authors [10—12] in the study of coherent apodization, the gradient of an edge image at the position $x = 0$ corresponding to the edge of an object is investigated by taking the first derivative of the edge image intensity, given by eq. (10), with respect to x and setting the resultant equation to be $x = 0$. This first derivative of eq. (10) yields after setting $x = 0$

$$D = \left.\frac{\partial I(x)}{\partial x}\right|_{x=0} = \frac{1}{2\pi}\int_{-1}^{1} T_0(u)\cos\{\Phi(u)\}du. \quad (12)$$

Equation (12) indicates that the gradient of the edge image is affected by both the amplitude transmittance $T_0(u)$ and the aberration $\Phi(u)$ of the optical imaging system. In order to reduce the edge shifting effect, it is desired that the integrated volume of eq. (12) must be made to be as large as possible for a given aberration $\Phi(u)$. This demand may be accomplished by controlling the amplitude transmittance $T_0(u)$ of the pupil, i.e. by introducing a proper apodized pupil function $T_0(u)$. In order to make the edge image approach faithfully to an original object, however, the edge ringing phenomenon should also be removed together with the reduction of edge shifting. This problem has already been studied in an aberration-free optical system by the present authors [11, 12] using the calculus of variations. In this paper,

the apodized pupil function $T_0(u)$ for removing or reducing the edge ringing phenomenon is investigated by considering the reduction of the edge shifting phenomenon when the optical imaging system has defocusing and primary spherical aberration.

In the present study the apodized pupil functions of three types are taken into consideration together with the non-apodized uniform function over the pupil. They are the triangular function, the function given by the autocorrelation of a cosine function, and the truncated Gaussian function which are expressed, respectively, by

$$T_{0r}(u) = \begin{cases} 1, & |u| \leqq 1 \\ 0, & |u| > 1 \end{cases} \tag{13a}$$

$$T_{0t}(u) = \begin{cases} 1-|u|, & |u| \leqq 1 \\ 0, & |u| > 1 \end{cases} \tag{13b}$$

$$T_{0c}(u) = \begin{cases} \dfrac{\sin(\pi|u|)}{\pi} + (1-|u|)\cos(\pi u), & |u| \leqq 1 \\ 0, & |u| > 1 \end{cases} \tag{13c}$$

$$T_{0g}(u) = \begin{cases} \exp(-\nu u^2), & |u| \leqq 1 \\ 0, & |u| > 1. \end{cases} \tag{13d}$$

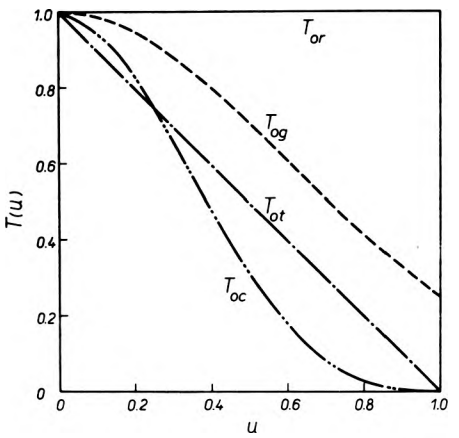

Fig. 1. Graphs of the apodized pupil functions $T_{0t}(u)$, $T_{0c}(u)$ and $T_{0g}(u)$ given by eqs. (13b), (13c) and (13d), while $T_{0r}(u)$ of eq. (13a) indicates the non-apodized pupil function

In eq. (13d), the constant ν is chosen to be $\exp(-\nu) = 0.25$. The pupil functions given by eq. (13) are shown in fig. 1. The non-apodized rectangular function of eq. (13a) is taken into consideration for comparison purpose. The physical meaning of the apodized pupil functions corresponding to eqs. (13b) and (13c) has been discussed in detail by ARAKI and ASAKURA [11]. Namely, the apodized pupil function of eq. (13b) is considered to minimize the edge shifting effect without the edge ringing phenomenon while that of eq. (13c) is to remove the edge ringing phenomenon on the basis of minimizing the second moment of the amplitude line spread function. These apodized pupil functions have been firstly proposed and used by SMITH, LEAVER and THOMPSON [3–6] to remove the edge ringing phenomenon. The truncated Gaussian apodized pupil function of eq. (13d) which is also considered to be very adequate for reducing the edge ringing phenomenon has been firstly proposed by THOMPSON and GRUBER [6, 7] and used by ASAKURA and ARAKI [10].

3. Apodized edge images in the presence of aberrations

3.1 Defocused edge images

We first study defocused edge images. For simple defocusing, the aberration function $\Phi(u)$ is described by

$$\Phi(u) = pu^2 \tag{14}$$

where p is the defocusing parameter showing the longitudinal displacement of the receiving plane from the Gaussian image plane. $p/2\pi$ is expressed in wavelength units. The intensity distribution of defocused edge images is now expressed from eqs. (10) and (14) as

$$I(x) = \left\{\frac{1}{2} + \frac{1}{2\pi}\int_{-1}^{1} T_0(u)\cos(pu^2)\frac{\sin(xu)}{u}\,du\right\}^2 + \left\{\frac{1}{2\pi}\int_{-1}^{1} T_0(u)\sin(pu^2)\frac{\sin(xu)}{u}\,du\right\}^2. \tag{15}$$

By substituting each of eq. (13) into eq. (15), the edge images corresponding to four forms of the pupil functions have been numerically evaluted by means of the Gauss quadrature method on an electronic computer and are shown in fig. 2. In this figure the defocusing parameter p is chosen as $p = 1.0$, 2.0, 3.0, 4.0, 5.0, 6.0 and 7.0. The non-apodized edge image of fig. 2(a) which have already been studied by BARAKAT [13] and ROWE [14] are highly sensitive to defocusing by which both edge ringing and shifting are strongly enhanced. On the other hand, figs. 2(b), (c) and (d) show that the apodized edge images less sensitive to defocusing than the non-apodized ones. Figure 2 indicates that the operation of apodization for reducing the edge ringing phenomenon is still useful in defocused edge images.

To evaluate the edge shift appearing in fig. 2, the first derivative of the edge image intensity with respect to x at the position $x = 0$ is taken and given

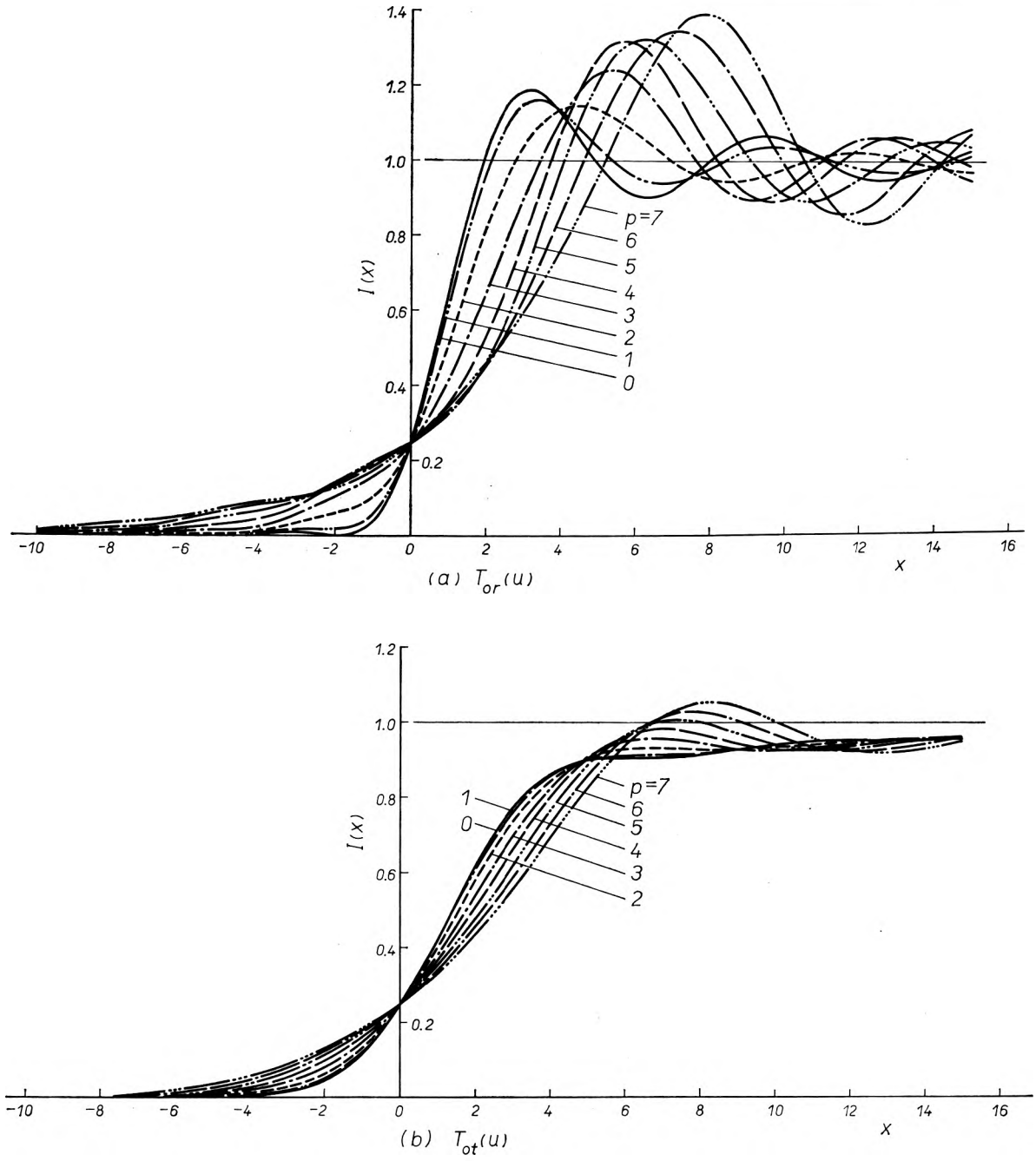

Fig. 2. Intensity distributions of non-apodized and apodized edge images obtained through an aberration-free defocuse apodized pupil function $T_{0t}(u)$, (c) the apodized pupil function

from eq. (12) as

$$D = \frac{\partial I(x)}{\partial x}\bigg|_{x=0} = \frac{1}{2\pi}\int_{-1}^{1} T_0(u)\cos(pu^2)du. \quad (16)$$

By substituting each of the functions given by eq. (13) into eq. (16), the first derivative D of the edge image at the position $x = 0$ is obtained as a function of the defocusing parameter p and shown in fig. 3 for the apodized pupil functions of three types together with the non-apodized case. This figure indicates that the first derivative of edge images for all apodized pupil functions given by eq. (13) monotonically decreases with the increase of defocusing from the Gaussian image plane. In other words, as the image plane is defocused from the Gaussian image plane, the gradient of edge images gradually decreases, the edge shift being consequently increased. On the other hand, the gradient of edge images tends to oscillate and has the second peak near point $p = 7.5$ for the non-apodized pupil. Since a decrease of the gradient as a function of the defocusing parameter p is relatively small for the apodized pupil functions in comparison

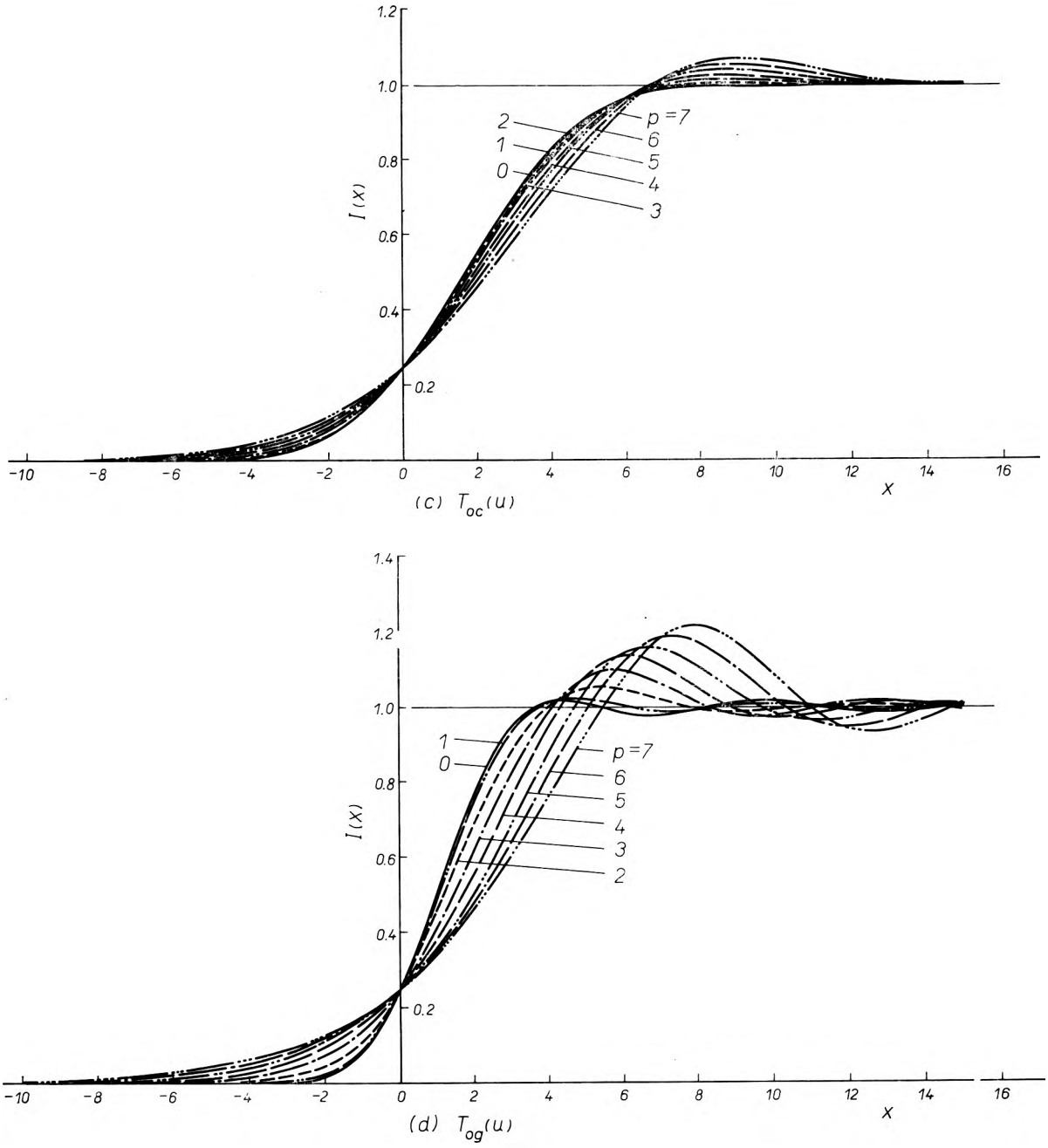

optical system. The defocusing parameter is indicated by pj (a) the non-apodized uniform pupil function $T_{0r}(u)$, (b) the $T_{0c}(u)$, (d) the apodized pupil function $T_{0g}(u)$

with that of the non-apodized case, edge images produced by using the apodized pupil functions employed to remove the edge ringing phenomenon is hardly affected by defocusing.

Figure 4 shows the actual edge shift E as a function of the defocusing parameter p. In this case, the edge shift E is defined by the distance from the object edge to the image edge at the intensity $I = 0.5$. Figure 4 has an inverse relation to fig. 3. This figure clearly indicates that the edge shift is largely produced for both non-apodized and apodized edge images with the increase of defocusing. But the increase of the edge shift is more rapid for the non-apodized pupil than that for the apodized pupils.

In order to indicate a degree of the edge ringing phenomenon, the first maximum intensity I_{max} of edge images is obtained as a function of the defocusing parameter p and shown in fig. 5. This figure shows how the edge ringing phenomenon is produced with the increase of defocusing. It becomes clear from figs. 2 and 5 that the apodized pupil function of eq. (13c) is very adequate for keeping edge images to have the least

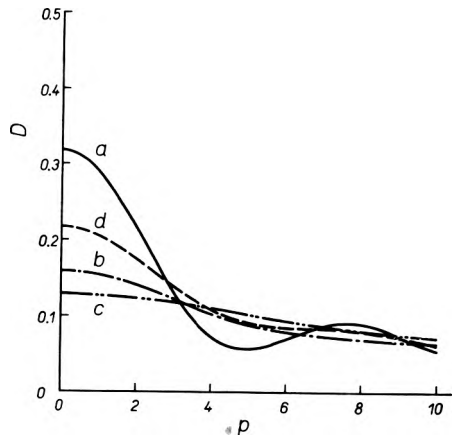

Fig. 3. Edge gradient D, defined by the first derivative of edge images at $x = 0$, as a function of the defocusing parameter p for the non-apodized pupil function $T_{0r}(u)$ (curve *a*) and the apodized pupil functions $T_{0t}(u)$ (curve *b*), $T_{0c}(u)$ (curve *c*), and $T_{0g}(u)$ (curve *d*)

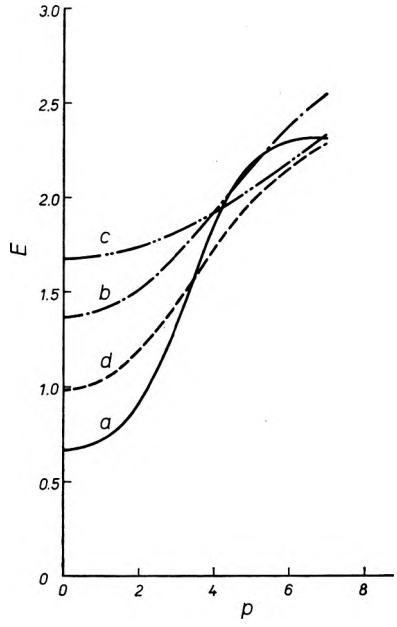

Fig. 4. Edge shift E of defocused edge images as a function of the defocusing parameter p for the non-apodized pupil function $T_{0r}(u)$ (curve *a*) and the apodized pupil functions $T_{0t}(u)$, $T_{0c}(u)$ and $T_{0g}(u)$ corresponding to the curves *b*, *c* and *d*

ringing phenomenon. Figures 4 and 5 suggest that the edge ringing effect is largely reduced even in defocused images by employing an apodized pupil function devised to remove the edge ringing phenomenon in focused images but the edge shifting effect is sensitively enhanced by defocusing even though the pupil is properly apodized.

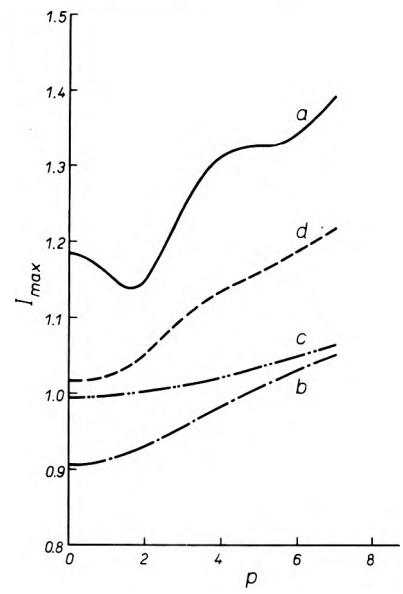

Fig. 5. First maximum intensity I_{max} of defocused edge images as a function of the defocusing parameter p for the non-apodized pupil function $T_{0r}(u)$ (curve *a*) and the apodized pupil functions $T_{0t}(u)$, $T_{0c}(u)$ and $T_{0g}(u)$ corresponding to the curves *b*, *c* and *d*

3.2 Apodized edge images in the presence of spherical aberration

When the coherent optical system has primary spherical aberration, the wave aberration function $\Phi(u)$ is described by

$$\Phi(u) = su^4 \tag{17}$$

and the pupil function of eq. (5) is expressed by

$$T(u) = T_0(u)\exp(isu^4) \tag{18}$$

where s is the primary spherical aberration coefficient, $s/2\pi$ being expressed in wavelength units.

By substituting eq. (18) into eq. (10) and again considering the non-apodized and apodized pupil functions of eq. (13), the aberrated edge images have been calculated by using an electronic computer and are shown in fig. 6. The primary spherical aberration coefficient s is chosen as $s = 1.0$, 2.0, 3.0, 4.0, 5.0, 6.0 and 7.0.

By substituting eq. (17) into eq. (12) and considering the pupil functions of four types given by eq. (13) for $T_0(u)$, the first derivative D of edge images at $x = 0$ is evaluated as a function of the spherical aberration coefficient s in order to show the edge gradient of aberrated edge images. The resultant values are plotted in fig. 7. Figures 8 and 9 show the edge shift and the first maximum intensity of aberrated edge images as a function of the primary spherical aberration coefficient s.

By comparing figs. 6, 7, 8 and 9 with figs. 2, 3, 4 and 5, the effects of primary spherical aberration in images of coherently illuminated edge objects are found to be qualitatively quite similar to those of defocusing but rather relatively weaker than those of defocusing. The detailed discussion on the results of figs. 6, 7, 8 and 9 is omitted since it is clear from the previous case 3.1 of defocusing.

3.3 Apodized edge images in the presence of defocusing and spherical aberration

When the coherent optical system holds a combined aberration of defocusing and primary spherical aberration, the wave aberration function $\Phi(u)$ may be expressed by

$$\Phi(u) = pu^2 + su^4. \tag{19}$$

It is well known in this case that there exists an optimum value p_0 of the defocusing parameter p for the given primary spherical aberration coefficient s in order to reduce the effect of a combined aberration on edge images. By considering the gradient of edge images at the position $x = 0$, the optimum value p_0 of defocusing is properly chosen which maximizes the gradient of edge images. The optical system set to have the optimum value p_0 of defocusing together with primary spherical aberration may be said to be at the aberration-balanced condition. This optimum value p_0 of defocusing is given as a solution of the following equation

$$\frac{\partial}{\partial p}\left[\frac{\partial I(x)}{\partial x}\bigg|_{x=0}\right] = -\frac{1}{2\pi}\int_{-1}^{1} u^2 T_0(u)\sin(pu^2+su^4)\,du = 0 \tag{20}$$

which has been obtained by substituting eq. (19) into eq. (12) and differentiating the resultant equation (12) with respect to p.

After substituting eq. (19) into eq. (12), the first derivative D of edge images at the position $x = 0$ has been numerically evaluated and is shown in fig. 10 as a function of the defocusing parameter p for the primary spherical aberration coefficient $s = -1.0, -2.0, -3.0, -4.0, -5.0, -6.0$ and -7.0 and for each of the pupil functions given by eq. (13). The optimum values p_0 of defocusing, which are obtained from eq. (20) and correspond to the maximum positions of p in fig. 10, for each of the primary spherical aberration coefficients are listed in table together with corresponding maximum edge gradients.

Optimum defocusing values p_0 and corresponding maximum edge gradients D for each of primary spherical aberration s and for the non-apodized and apodized pupil functions of $T_{0r}(u)$, $T_{0t}(u)$, $T_{0c}(u)$ and $T_{0g}(u)$

(a) $T_{0r}(u)$

s	p_0	D
0	0	0.3183
−1	0.714	0.3169
−2	1.425	0.3126
−3	2.131	0.3056
−4	2.829	0.2960
−5	3.512	0.2841
−6	4.174	0.2703
−7	4.800	0.2551

(b) $T_{0t}(u)$

s	p_0	D
0	0	0.1592
−1	0.535	0.1589
−2	1.066	0.1582
−3	1.587	0.1570
−4	2.092	0.1554
−5	2.576	0.1535
−6	3.031	0.1513
−7	3.445	0.1490

(c) $T_{0c}(u)$

s	p_0	D
0	0	0.1290
−1	0.357	0.1290
−2	0.712	0.1288
−3	1.062	0.1286
−4	1.402	0.1283
−5	1.739	0.1279
−6	2.061	0.1275
−7	2.371	0.1270

(d) $T_{0g}(u)$

s	p_0	D
0	0	0.2166
−1	0.644	0.2159
−2	1.284	0.2140
−3	1.913	0.2107
−4	2.524	0.2064
−5	3.107	0.2011
−6	3.646	0.1951
−7	4.108	0.1888

Figure 10 (a) together with table indicates that in the case of the non-apodized pupil function the optimum receiving plane designated by the optimum defocusing parameter p_0 gradually departs from the Gaussian image plane $p = 0$ with the increase of primary spherical aberration s and that the edge gradient rapidly decreases with the increase of separation of the receiving plane from the optimum receiving plane defined by p_0. Furthermore, the maximum gradient at the optimum receiving plane is found in fig. 10 (a) to gradually decrease with the increase of spherical aberration in the case of the non-apodized pupil function $T_{0r}(u)$.

As is clear from fig. 10 (b) –(d), the above phenomenon is similarly observed for the apodized pupil functions. But a change of the edge gradient D as a function of defocusing p from the optimum receiving plane p_0 is small in comparison with the case of the non-apodized pupil function. This point is especially remarkable for the apodized pupil function $T_{0c}(u)$. In addition, the decrease of the maximum gradient with the increase of the spherical aberration coefficient s is also not so recognizable that the

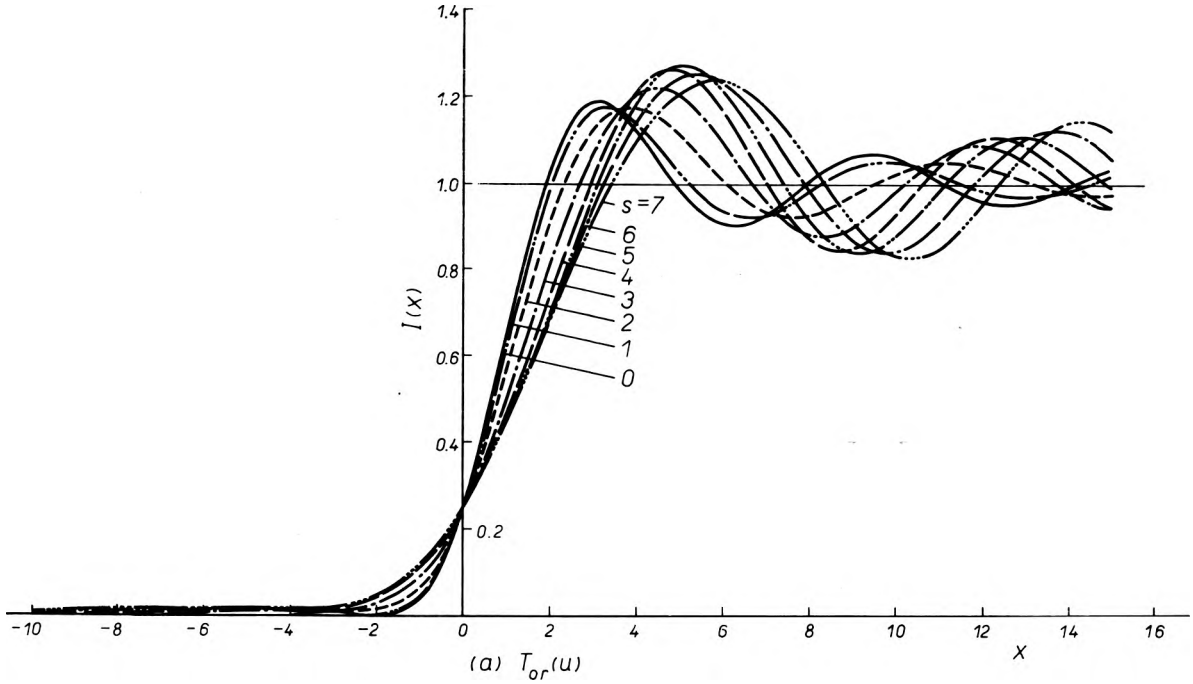

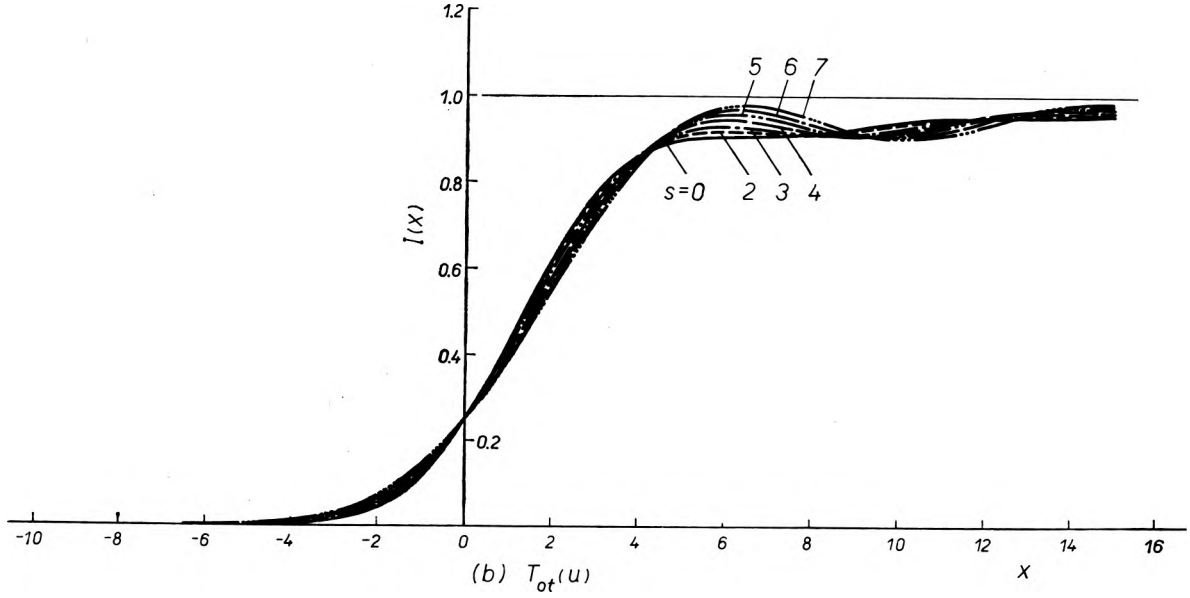

Fig. 6. Intensity distributions of non-apodized and apodized edge images obtained through an optical system (a) The non-apodized pupil function $T_{0r}(u)$, (b) the apodized pupil function $T_{0f}(u)$,

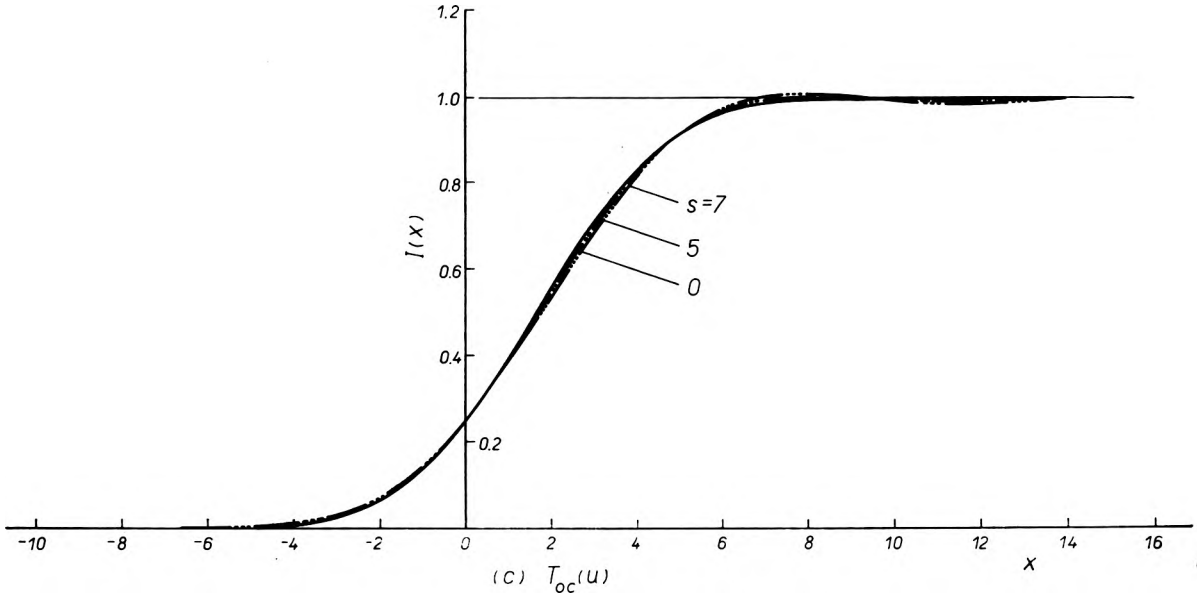

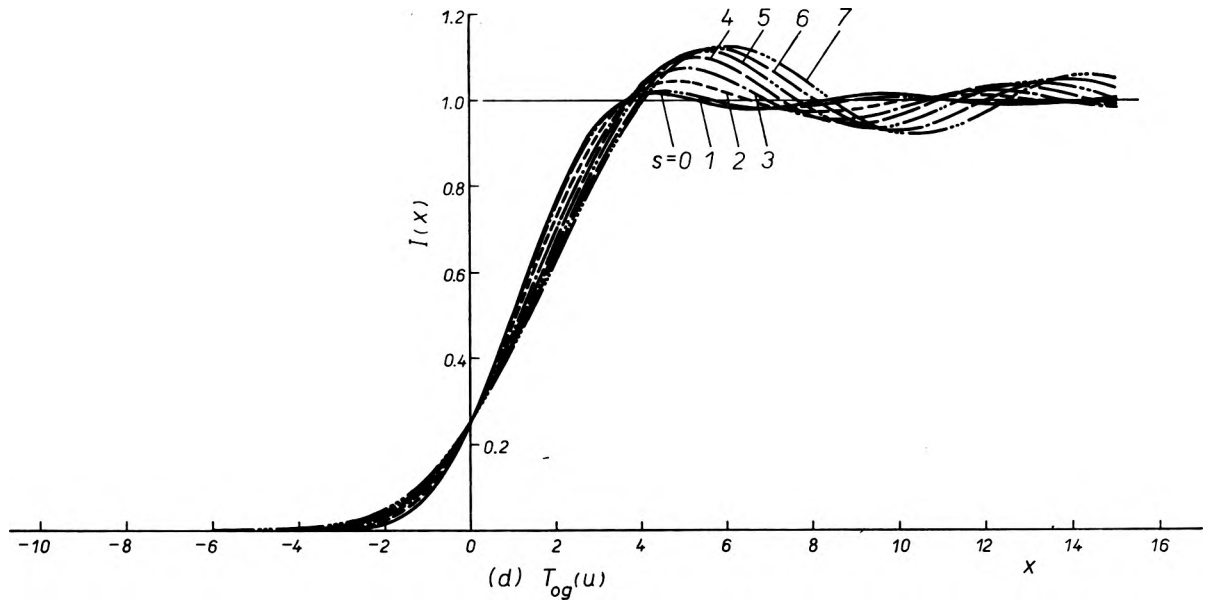

having primary spherical aberration. The spherical aberration coefficient is indicated by s
(c) the apodized pupil function $T_{0c}(u)$, and (d) the apodized pupil function $T_{0g}(u)$

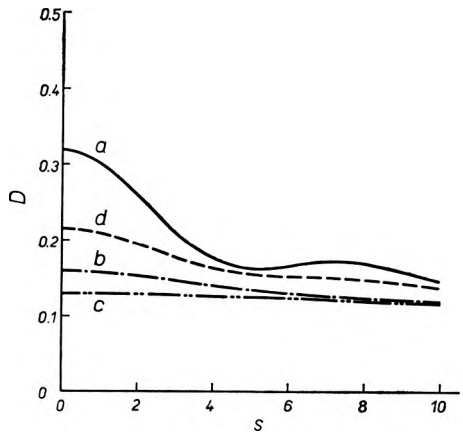

Fig. 7. Edge gradient D as a function of the primary spherical aberration coefficient s for the non-apodized pupil function $T_{0r}(u)$ (curve *a*) and the apodized pupil functions $T_{0t}(u)$ (curve *b*), $T_{0c}(u)$ (curve *c*), and $T_{0g}(u)$ (curve *d*)

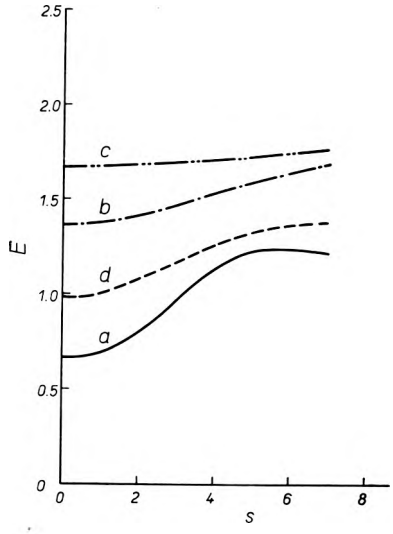

Fig. 8. Edge shift E as a function of the primary spherical aberration coefficient s for the non-apodized pupil function $T_{0r}(u)$ (curve *a*) and the apodized pupil functions $T_{0t}(u)$, $T_{0c}(u)$ and $T_{0g}(u)$ corresponding to the curves *b*, *c* and *d*

effect of spherical aberration on the edge gradient at the optimum receiving plane is very small.

By giving the values p_0 of the optimum receiving plane in table, corresponding to each of s, for p in eq. (19) and substituting the resultant equation (19) into eq. (10), the intensity distributions of edge images in the presence of primary spherical aberration produced at the optimum receiving plane have been evaluated on an electronic computer but are not shown here because they are almost similar to edge images of figs. 2 and 6 corresponding to $p = 0$ and $s = 0$ without regard to the value of spherical aberration s. The resultant edge images clearly indicate that there appears almost no increases of the edge shift at the optimum receiving planes with the increase

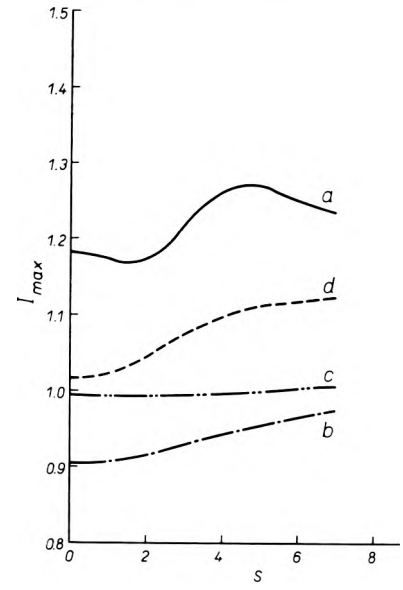

Fig. 9. First maximum intensity I_{max} of aberrated edge images as a function of the primary spherical aberration coefficient s for the non-apodized pupil function $T_{0r}(u)$ (curve *a*) and the apodized pupil functions $T_{0t}(u)$, $T_{0c}(u)$ and $T_{0g}(u)$ corresponding to the curves *b*, *c* and *d*

of spherical aberration s even though a very slight shift is recognized only in the cases of the non-apodized pupil function $T_{0r}(u)$ and the apodized pupil function $T_{0g}(u)$. In the optical imaging system having a combined aberration of defocusing and primary spherical aberration, therefore, the apodization of reducing the edge ringing phenomenon without the increase of the edge shift is possible at the optimum receiving plane by employing a proper apodized pupil function.

In fig. 11, the first maximum intensity I_{max} of edge images produced at the optimum receiving planes is shown as a function of the primary spherical aberration coefficient s. This figure indicates that in the case of the apodized pupil functions (refer to the curves *b*, *c* and *d*) the first maximum intensity does not vary by increasing spherical aberration while it gradually decreases in the case of the non-apodized pupil function (see the curve *a*).

Finally, the edge shift E is shown fig. 12 for edge images produced at the optimum receiving planes, as a function of primary spherical aberration s. It is seen from this figure that there appears almost no increase of the edge shift in edge images produced at the optimum receiving planes.

4. Conclusion

This paper may the first contribution to the study on apodized images of coherently illuminated edges in the presence of defocusing and primary

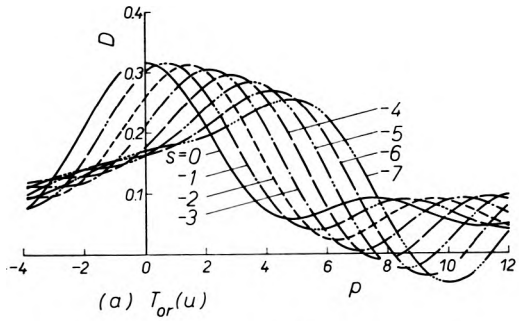

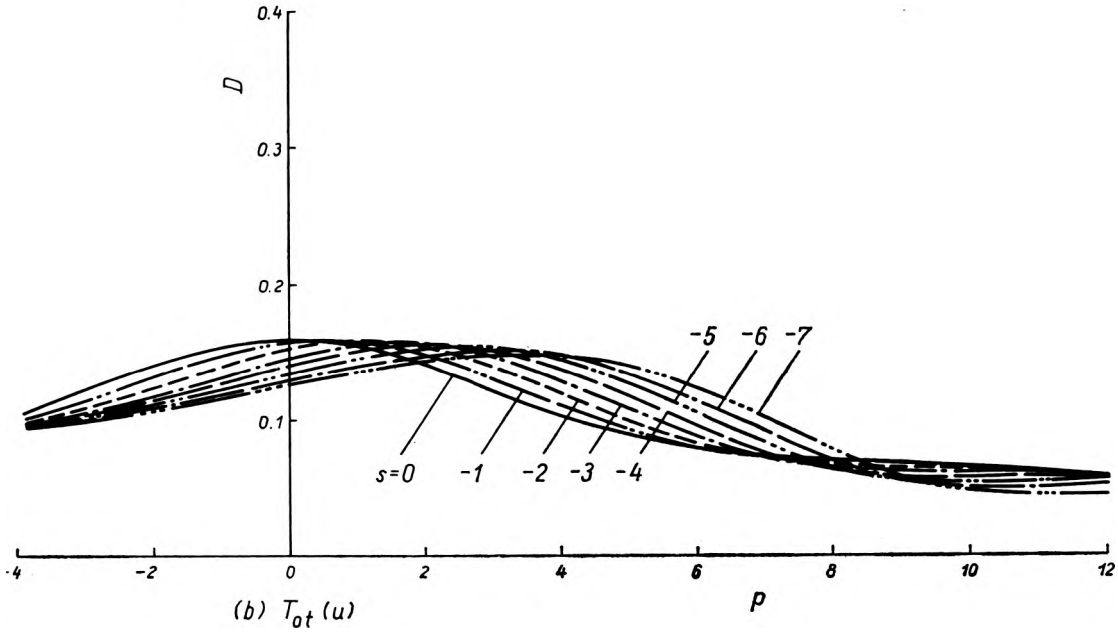

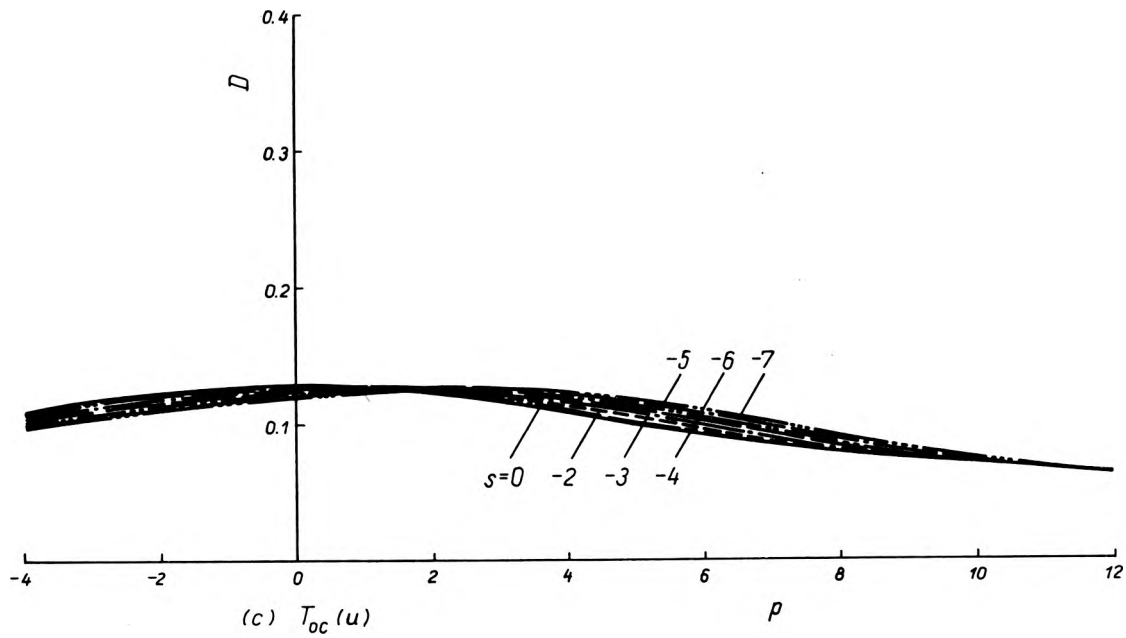

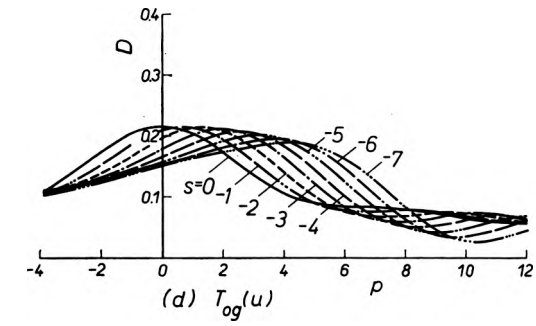

Fig. 10. Edge gradient D of aberrated edge images as a function of the defocusing parameter p for each of the primary spherical aberration coefficients s

(a) The non-apodized pupil function $T_{0r}(u)$ (figure (a)) and the apodized pupil functions $T_{0t}(u)$, $T_{0c}(u)$ and $T_{0g}(u)$ corresponding to the figures (b), (c) and (d)

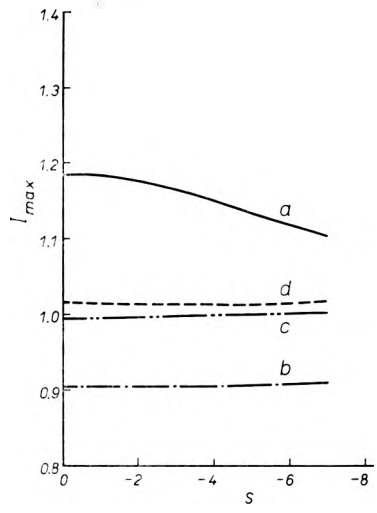

Fig. 11. First maximum intensity I_{max} of non-apodized and apodized edge images obtained at the optimum defocused receiving planes p_0 through an optical system having primary spherical aberration s. Curves a, b, c and d correspond to the non-apodized pupil function $T_{0r}(u)$ and the apodized pupil functions $T_{0t}(u)$, $T_{0c}(u)$ and $T_{0g}(u)$

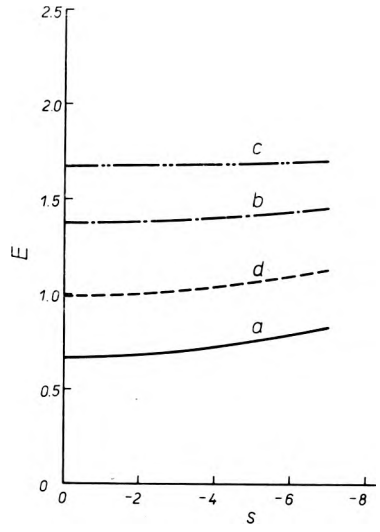

Fig. 12. Edge shift E of non-apodized and apodized edge images obtained at the optimum defocused receiving planes p_0 through an optical system having primary spherical aberration s. Curves a, b, c and d correspond to the non-apodized pupil function $T_{0r}(u)$ and the apodized pupil functions $T_{0t}(u)$, $T_{0c}(u)$ and $T_{0g}(u)$

spherical aberration in coherent optical systems. The edge ringing and shifting phenomena are increased with the increase of defocusing in both cases of the non-apodized and apodized pupil functions. The non-apodized images are highly sensitive to defocusing by which the above two phenomena are strongly enhanced, while the apodized edge images are less sensitive to defocusing than the non-apodized ones. Therefore, the apodization is useful for reducing these two phenomena even in defocused edge images.

The effect of primary spherical aberration in non-apodized and apodized edge images are qualitatively similar to those of defocusing but rather weaker than those of defocusing.

When the optical imaging system holds both defocusing and primary spherical aberration, there is an optimum receiving plane at which the edge shifting takes a minimum and the effect of apodization for reducing or removing the edge ringing phenomenon is effectively produced similarly to the case of the aberration-free optical system.

The present study may be worthwhile for designing coherent optical systems employing lasers as light sources since various techniques employing coherent optical systems are expected to be popular.

Аподизированные изображения когерентно освещенных границ расфокусировки и сферической аберрации

Исследованы аподизированные изображения границ, когерентно освещенных при наличии расфокусировки и первичной сферической аберрации для трех видов аподизационных зрачков по сравнению с неаподизированными изображениями границ. Полученные аподизированные изображения оценивались на основе интерференционных явлений и смещения границ, происходящих обычно в каждом изображении границы, когерентно освещенной без аподизации.

References

[1] Considine P. S., J. pt. Soc. Am. **56**, 8, 1001 (1966).
[2] Smith R. W., Opt. Commun. **4**, 157 (1971).
[3] Smith R. W., Opt. Commun. **6**, 1, 8 (1972).
[4] Smith R. W., Opt. Commun. **9**, 1, 61 (1973).
[5] Leaver F. G., Smith R. W., Optik **39**, 2, 156 (1973).
[6] Thompson B. J, *Image Assessment and Specification*, ed. by D. Dutton, SPIE Publications, 1974, p. 27.
[7] Gruber L. S., Thompson B. J., Opt. Eng. **13**, 5, 451 (1974).
[8] Leaver F. G., Opt. Commun. **15**, 3, 370 (1975).
[9] Leaver F. G., Smith R. W., Opt. Commun. **15**, 3, 374 (1975).
[10] Asakura T., Araki T., Optik **46**, 4, 365 (1976).
[11] Araki T., Asakura T., Opt. Commun. **20**, 3, 373 (1977).
[12] Araki T., Asakura T., to be submitted for publication.
[13] Barakat R., Optica Acta **16**, 2, 205 (1969).
[14] Rowe S. H., J. opt. Soc. Am. **59**, 6, 711 (1969).
[15] Thompson B. J., *Progress in Optics*, ed. by E Wolf, North-Holland Publ. Amsterdam 1969, p. 168.

Received, April 10, 1978